

Transport in polymer-gel composites: Theoretical methodology and response to an electric field

By REGHAN J. HILL

Department of Chemical Engineering and McGill Institute for Advanced Materials, McGill
University, Montreal, Quebec, H3A2B2, CANADA

(Received 8 February 2020)

A theoretical model of electromigrative, diffusive and convective transport polymer-gel composites is presented. Bulk properties are derived from the standard electrokinetic model with an impenetrable charged sphere embedded in an electrolyte-saturated Brinkman medium. Because the microstructure can be carefully controlled, these materials are promising candidates for enhanced gel-electrophoresis, chemical sensing, drug delivery, and microfluidic pumping technologies. The methodology provides ‘exact’ solutions for situations where perturbations from equilibrium are induced by gradients of electrostatic potential, concentration and pressure. While the volume fraction of the inclusions should be small, Maxwell’s well-known theory of conduction suggests that the theory may also be accurate at moderate volume fractions. In this work, the model is used to compute ion fluxes, electrical current density, and convective flow induced by an applied electric field. The electric-field-induced (electro-osmotic) flow is a sensitive indicator of the inclusion ζ -potential and size, electrolyte concentration, and Darcy permeability of the gel, while the electrical conductivity increment is most often independent of the polymer gel, and is much less sensitive to particle and electrolyte characteristics.

CONTENTS

1. Introduction	2
2. Theory	4
2.1. The electrokinetic transport equations	7
2.2. Solution of the equations	8
2.3. Averaged (bulk) fluxes	11
2.4. Averaged (bulk) momentum conservation equations	13
2.5. Averaged (bulk) equations for unidirectional transport	14
3. Response to an electric field	15
3.1. Incremental pore velocity	15
3.2. Electroosmotic pumping	19
3.3. Incremental pressure gradient	22
3.4. Species fluxes	22
3.5. Electrical conductivity	23
4. Summary	26

1. Introduction

Gel-electrophoresis is widely used to sort macromolecules based on their size and electrical charge. Selectivity to size is achieved by adjusting the permeability of the gel (*e.g.*, agarose or polyacrylamide) through the concentrations of monomer, cross-linker, catalyst and initiator used in the gel synthesis. Molecular sorting based on other characteristics, such as receptor-ligand binding affinity, requires the gel to exhibit specific physiochemical activity. One way to achieve this in a controlled manner is to embed surface-functionalized particles (*e.g.*, cells or synthetic polymer or silica spheres) in a “conventional” polymer gel. Accordingly, this work seeks to quantify the influence of surface charge on transport driven by gradients of chemical and electrostatic potential. While the task is simplified to some extent by limiting the analysis to simple electrolytes whose mobilities are unhindered by the polymer gel, the methodology provides a significant step toward a theory that also accounts for hindered transport of larger electrolyte ions (*e.g.*, proteins and DNA fragments).

This work also provides a quantitative interpretation of novel diagnostic tests—analogueous to well-established microelectrophoresis and conductivity measurements—that probe the surface charge or ζ -potential of immobilized colloids in electrolytes where the particles would otherwise aggregate. Attractive particle-interaction potentials arise when the solution pH approaches the isoelectric point of the particle-electrolyte interface, or the surface charge is sufficiently well screened by added salt (Russel *et al.* 1989). By immobilizing colloids in an (ideally) inert (uncharged) polymer gel, at a pH and ionic strength where the interactions are repulsive, the pH and ionic strength may be varied without inducing coagulation.

Membranes of sintered glass beads (without intervening polymer) have long been used in ion-selective electrodes, and, more recently, as electroosmotic pumps (*e.g.*, Yao *et al.* 2003). Their simple design (no moving parts) and high-pressure, low-flow characteristics are ideally suited to microfluidic applications. Filling the void space with a permeable, uncharged polymer gel, as proposed in this work, will increase viscous dissipation and, therefore, diminish pumping efficiency. Nevertheless, because applications are envisioned where poor pumping efficiency might be tolerated in view of other novel attributes, a quantitative analysis of electroosmotic pumping is undertaken here.

The charge on particles dispersed in an electrolyte endows them with an electrophoretic mobility (Russel *et al.* 1989). Theoretical interpretation of the mobility (O’Brien & White 1978), sedimentation potential (Saville 1982), low-frequency conductivity (Saville 1979; O’Brien 1981), dielectric response (complex conductivity) (DeLacey & White 1981), and electroacoustic response (dynamic mobility) (O’Brien 1988, 1990) is widely used to infer the surface charge and, therefore, to indicate dispersion stability. Closely related are streaming-potential and streaming-current devices, which are used to infer the charge on macroscopic substrates, and the charge density and permeability of porous plugs and coatings (*e.g.*, Hunter 2001; Dukhin *et al.* 2004).

This paper addresses a new but related problem in which impenetrable spheres with surface charge are randomly dispersed and immobilized in a permeable, electrolyte-saturated polymer gel (see figure 1). The transport processes that take place with the application of average (macroscale) gradients of electrostatic potential, electrolyte concentration and pressure are derived. While transport of electrolyte ions is relatively straightforward to calculate in an homogeneous, uncharged gel, charged inclusions disturb the applied fields, and applied fields disturb the equilibrium state of the diffuse double layers, so the resulting fluxes reflect a complex coupling of electromigrative, diffusive and convective transport.

Electrokinetic theories are often based on the *standard electrokinetic model* (Booth 1950), whereby continuum equations governing the electric field, mobile charge (microions), mass and momentum are solved with appropriate boundary conditions. The principal difficulty usually lies in capturing double-layer polarization and relaxation at surfaces whose radius of curvature is comparable to or smaller than the equilibrium double-layer thickness (Debye length). For ‘bare’ and ‘soft’ (polymer-coated) particles, polarization and relaxation can be addressed with novel numerical methodologies (O’Brien & White 1978; Hill *et al.* 2003). In this work, a numerically exact solution of the problem is achieved for the low-volume-fraction limit where particle interactions can be neglected. The methodology also neglects quadratic and higher-order perturbations to the equilibrium state, providing *asymptotic coefficients* that characterize the far-field (power-law) decays of the velocity disturbance, and perturbations to the equilibrium electric field and ion concentrations. In turn, the asymptotic coefficients are linked to bulk properties of the composite. The analysis resembles Maxwell’s theory for effective conductivity of a dilute, random configuration of spherical inclusions.

Dipolar disturbances[†] arise in the limit where the inclusions are uncharged. Then, with the application of a uniform electric field, the perturbed electrostatic potential ψ' reflects the non-conducting (impenetrable) surface of the inclusions, satisfying $\nabla^2\psi' = 0$. Similarly, when subjected to a bulk concentration gradient, the perturbed ion concentrations n' satisfy $\nabla^2 n' = 0$. In both cases, there is no convective flux, because the electrolyte is everywhere electrically neutral. With a uniform pressure gradient $\langle \nabla p \rangle$, the problem simplifies to the flow of an incompressible Newtonian fluid through a Brinkman medium with impenetrable inclusions. The (solenoidal) velocity \mathbf{u} satisfies $\eta \nabla^2 \mathbf{u} - \nabla p - (\eta/\ell^2)\mathbf{u} = \mathbf{0}$, where p is the pressure, η is the fluid viscosity, and ℓ is the Brinkman screening length (square root of the Darcy permeability). When the inclusion radius $a \gg \ell$, $\mathbf{u} = -(\ell^2/\eta)\nabla p$ with $\nabla^2 p = 0$ (Darcy flow), and the drag force on the inclusions is $2\pi\eta U a^3 \ell^{-2}$, where $\mathbf{U} = -\langle \nabla p \rangle \ell^2/\eta + O(\phi)$ is the average fluid velocity. In this limit, the inclusion contribution to the average drag force (per unit volume) of the *composite* is $2\pi n \eta U a^3 \ell^{-2} = (3/2)\phi \eta \mathbf{U} \ell^{-2}$, where n is the inclusion number density and $\phi = n(4/3)\pi a^3$ the volume fraction. With the same far-field velocity, the drag on each inclusion is clearly much larger than the Stokes drag force $6\pi\eta a \mathbf{U}$. Note also that the velocity disturbances $\mathbf{u}' = \mathbf{u} - \mathbf{U} = -(1/2)a^3 U_j (\delta_{ij} r^{-3} - 3x_i x_j r^{-5})$ decay as r^{-3} when the distance from the inclusions $r \gg a \gg \ell$.

When the inclusions are charged, a diffuse layer of mobile counterions envelopes each inclusion, and electroneutrality demands that the net charge in the diffuse layers balances the immobile surface charge. With an applied electric field, the electrical body force within the diffuse layers drives an ‘inner’ flow which, in turn, drives an $O(\phi)$ ‘outer’ flow, with an $O(1)$ contribution due to an imposed pressure gradient. The electric-field-induced velocity disturbances ‘pump’ fluid through the polymer gel without exerting a net force on the composite. While the velocities are very low, composites with an a 1 cm² cross-section can produce velocities of several microns per second in a microchannel. Note that a pressure gradient is necessary to overcome the drag required to pump fluid through an external network. However, the pressure-driven contribution to the flow is often small compared to the electric-field-induced flow. Under these conditions, the electric-field-induced flow rate is practically independent of the pressure gradient, and the maximum

[†] Here, *dipolar* refers to axis-symmetric disturbances, without a source, that satisfy Laplace’s equation; these take the form $\alpha_j \partial r^{-1} / \partial x_j = -\alpha_j x_j r^{-3}$, where $r = |\mathbf{x}|$ and α_i are the components of a constant vector.

pressure gradient that can be sustained is limited by the strength of the composite and its support.

Ion fluxes manifest in an electrical current and, hence, a measurable *electrical conductivity*. Following earlier treatments of the low-frequency conductivity of dilute colloidal dispersions (Saville 1979; O’Brien 1981), the incremental contribution of the inclusions to the effective conductivity is calculated. These results link conductivity measurements to the particle surface charge density, for example. Because the fluxes are dominated by electromigration, the conductivity is not significantly influenced by the gel.

The model also provides the effective diffusivities of electrolyte ions when the bulk electrolyte concentration varies slowly in space and time. In an accompanying paper, two important situations are examined: (i) bulk diffusion in the absence of an average electric field, and (ii) bulk diffusion with an electric field yielding zero current density. The former provides a simple setting in which to demonstrate the extent to which inclusions change the effective ion diffusion coefficients, whereas the latter provides the particle contribution to the *membrane diffusion potential*, which is well known in the fields of membrane biology, electrochemistry, and electrochemical engineering. In both cases, the particle contribution to these bulk properties may be comparable or larger than in the absence of inclusions.

The paper is organized as follows. We begin in §2 with a description of the electrokinetic model. First, the composite microstructure and an apparatus for comparing theory and experiment are described. The subsections therein present the electrokinetic transport equations (§2.1), which are used to compute linearly independent solutions of the single-particle (microscale) problem (§2.2). Asymptotic coefficients from ‘exact’ solutions of the microscale problem capture far-field decays of perturbations to the equilibrium state. These are used to calculate bulk ion fluxes in §2.3, and to derive an average momentum equation in §2.4. Results are presented in §3 for composites with negatively charged inclusions in polymer gels saturated with NaCl electrolyte. The subsections therein examine the incremental pore mobility (§3.1), electroosmotic pumping (§3.2), incremental pressure gradient (§3.3) and, finally, species fluxes (§3.4) and electrical conductivity (§3.5). A brief summary follows in §4.

2. Theory

The microstructure of the composites addressed in this work is depicted schematically in figure 1. The continuous phase is a porous medium comprised of an electrically neutral, electrolyte-saturated polymer gel[†]. Polyacrylamide gels are routinely used for the electrophoretic separation of DNA segments in aqueous solution. Their porosity may be controlled by adjusting the average densities and ratio of the monomer (acrylamide) and cross-linker. In this work, the hydrodynamic permeability is characterized by the Darcy permeability ℓ^2 (square of the Brinkman screening length), which reflects the hydrodynamic size a_s and concentration n_s of the polymer segments. In turn, these reflect the degree of cross-linking and the affinity of the polymer for the solvent.

Embedded in the polymer are randomly dispersed spherical inclusions. In model systems, these are envisioned to be monodisperse silica or polymeric spheres, which typically have radii in the range $a = 10 \text{ nm} - 10 \text{ }\mu\text{m}$ and bear a surface charge when dispersed in aqueous media. The surface charge density may vary with the bulk ionic strength and pH of the electrolyte. In this work, however, the surface charge is to be inferred from

[†] A *gel* refers to a network of polymer chains that is cross-linked so as to exhibit a solid-like (elastic) response to an applied stress.

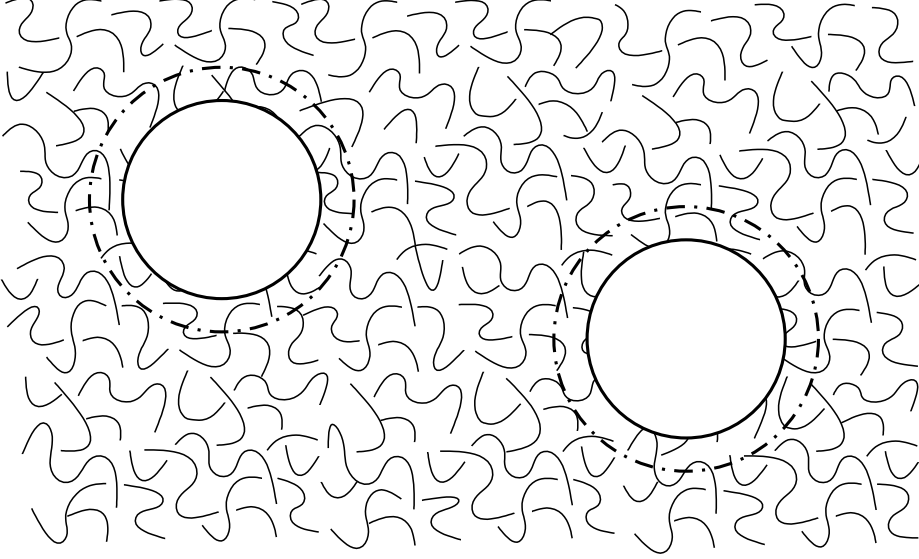


FIGURE 1. Schematic of the *microscale* system under consideration. Charged, impenetrable inclusions (*solid circles*) with radius $a \sim 10 \text{ nm} - 10 \text{ }\mu\text{m}$ are embedded in a continuous polymer gel (*solid filaments*) saturated with aqueous electrolyte. Equilibrium diffuse double layers (*dash-dotted circles*) with thickness $\kappa^{-1} \sim 1 - 100 \text{ nm}$ are perturbed by the application of an average electric field $-\langle \nabla \psi \rangle$, pressure gradient $\langle \nabla p \rangle$, or electrolyte concentration gradient $\langle \nabla n_j \rangle$. The Brinkman screening length $\ell \sim 1 - 10 \text{ nm}$ that specifies the Darcy permeability ℓ^2 of the gel is often small compared to the radius a of the inclusions.

the bulk ionic strength and surface potential ζ . Because the inclusions are impenetrable with zero surface capacitance and conductivity, no-flux and no-slip boundary conditions apply at their surfaces.

Note that the mobile ions whose charge is opposite to the surface-bound, immobile charge are referred to as *counterions*, with the other species referred to as *co-ions*. For simplicity, the counter-charges, *i.e.*, the dissociated counterions, are assumed indistinguishable from the electrolyte counterions. Surrounding each inclusion is a diffuse layer of mobile charge, with Debye thickness κ^{-1} and excess of counterions. This is referred to as the equilibrium diffuse double layer, and, as described below, its structure is calculated from the well-known Poisson-Boltzmann equation.

In this work, the polymer gel is assumed not to hinder ion motion. For larger ions and dense polymer gels, the influence of the network on the diffusive, electromigrative and convective fluxes may be modeled with an equation of motion for an ion

$$\gamma(\mathbf{u} - \mathbf{v}) - \gamma'\mathbf{v} + \mathbf{f} = \mathbf{0}, \quad (2.1)$$

where the first term represents the hydrodynamic drag due to relative motion; \mathbf{u} and \mathbf{v} are, respectively, the (average) fluid and ion velocities, with γ the friction coefficient. The second term approximates the force exerted by the polymer gel on the ion, where the friction coefficient γ' reflects the relative size of the ion and polymer interstices. The third term accounts for electrical and thermal (Brownian) forces, depending on the time-scale of interest. The unhindered ion velocity is $\mathbf{v}^0 = \mathbf{u} + \mathbf{f}/\gamma$, so the hindered velocity may be written $\mathbf{v} = \mathbf{v}^0\gamma/(\gamma + \gamma')$. Therefore, under steady conditions, the ion conservation equation $\nabla \cdot (n\mathbf{v}) = 0$ is independent of γ' (n is the ion number density). When $\mathbf{u} = \mathbf{0}$, for example, the ion will diffuse (or electromigrate) with an *effective* diffusivity (or mobility) $D^e = D\gamma/(\gamma + \gamma')$, where D is the unhindered diffusivity. It follows that $\mathbf{v} = \mathbf{v}^0 D^e/D$,

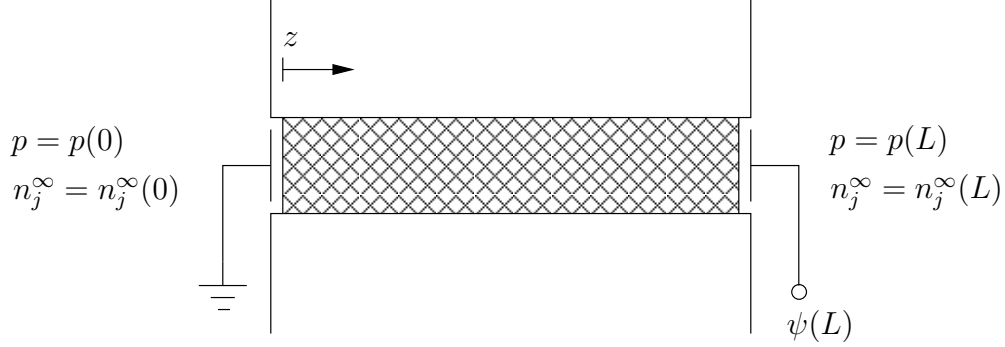


FIGURE 2. Schematic of the *macroscale* system under consideration. A polymer gel embedded with spherical charged inclusions (see figure 1) separates (by length L) two reservoirs containing electrolyte with different species concentrations ($n_j^\infty(z=0)$ and $n_j^\infty(z=L)$) and, possibly, pressures ($p(z=0)$ and $p(z=L)$). Electrodes on each side of the ‘bridge’ permit an electric field to be applied and the differential electrostatic potential $\Delta\psi = \psi(z=L) - \psi(z=0)$ to be measured. The walls of the bridge are impenetrable and non-conducting.

so the hindered flux equals the unhindered flux multiplied by the ratio of the hindered to unhindered ion diffusivities (mobilities).

Now consider the influence of hindered ion migration on the fluid momentum conservation equation. From Eqn. (2.1), the (hydrodynamic drag) force exerted by an ion on the solvent is

$$\gamma(\mathbf{v} - \mathbf{u}) = (\mathbf{f} - \gamma'\mathbf{u})\gamma/(\gamma + \gamma'), \quad (2.2)$$

where $\mathbf{f} = -ze\nabla\psi$ is the electrical force on the ion (z is the valance, e is the elementary charge, and ψ is the electrostatic potential). It follows that the net force (per unit volume) exerted on the fluid by the ions is

$$-\sum_{j=1}^N n_j(\gamma'_j\mathbf{u} + z_j e \nabla\psi) D_j^e / D_j, \quad (2.3)$$

where the sum is over all N ion species. Clearly, in the limit $\gamma'_j/\gamma_j \rightarrow 0$ where the hindrance of the polymer is negligible, ions transfer their electrical force to the fluid. In the limit $\gamma'_j/\gamma_j \rightarrow \infty$, however, immobilized ions transfer the electrical force to the polymer, so the net force exerted by each ion on the fluid becomes $-\gamma_j\mathbf{u}$.

A simple apparatus that, in principle, could be used to realize the conditions under which the theory may be applied is depicted in figure 2. The composite bridges two reservoirs, each, in general, with a different electrolyte concentration and pressure. Electrodes are placed at each end of the bridge, so either a uniform electric field can be established or an average electric field strength measured. The channel is to realize constant ion fluxes under steady or quasi-steady conditions. This makes the averaged microscale transport equations easier to solve, but, in general, the averaged equations apply to macroscale fluxes in two- and three-dimensional geometries when the (average) inclusion number density, ion concentrations, electric field and fluid velocity vary slowly in space and time.

2.1. The electrokinetic transport equations

The transport equations and boundary conditions are presented here in dimensional form. They comprise the non-linear Poisson-Boltzmann equation,

$$\epsilon_o \epsilon_s \nabla^2 \psi = - \sum_{j=1}^N (n_j - n_j^f) z_j e, \quad (2.4)$$

where ϵ_o and ϵ_s are the permittivity of a vacuum and dielectric constant of the electrolyte; n_j and n_j^f are the concentrations of the j th mobile and fixed charges, with z_j the valences[†]; e is the elementary charge and ψ the electrostatic potential. In this work, the polymer is uncharged, so $n_j^f = 0$.

Transport of the mobile ions is governed by

$$6\pi\eta a_j (\mathbf{u} - \mathbf{v}_j) - z_j e \nabla \psi - kT \nabla \ln n_j = 0 \quad (j = 1, \dots, N), \quad (2.5)$$

where a_j are Stokes radii of the ions, obtained from limiting conductances or diffusivities; η is the electrolyte viscosity, \mathbf{u} and \mathbf{v}_j are the fluid and ion velocities, and kT is the thermal energy. Ion diffusion coefficients, which are adopted below, are

$$D_j = kT / (6\pi\eta a_j). \quad (2.6)$$

As usual, the double-layer thickness (Debye length)

$$\kappa^{-1} = \sqrt{kT \epsilon_s \epsilon_o / (2I e^2)} \quad (2.7)$$

emerges from Eqns. (2.4) and (2.5) where

$$I = (1/2) \sum_{j=1}^N z_j^2 n_j^\infty \quad (2.8)$$

is the bulk (average) ionic strength, with n_j^∞ the bulk ion concentrations.

Ion conservation demands

$$\partial n_j / \partial t = -\nabla \cdot (n_j \mathbf{v}_j) \quad (j = 1, \dots, N), \quad (2.9)$$

where t is the time and the ion fluxes $\mathbf{j}_j = n_j \mathbf{v}_j$ are obtained from Eqn. (2.5).

Similarly, momentum and mass conservation require

$$\rho_s \partial \mathbf{u} / \partial t = \eta \nabla^2 \mathbf{u} - \nabla p - (\eta / \ell^2) \mathbf{u} - \sum_{j=1}^N n_j z_j e \nabla \psi \quad (2.10)$$

and

$$\nabla \cdot \mathbf{u} = 0, \quad (2.11)$$

where ρ_s and \mathbf{u} are the electrolyte density and velocity, and p is the pressure. Note that $-(\eta / \ell^2) \mathbf{u}$ represents the hydrodynamic drag force exerted by the polymer on the electrolyte, with ℓ^2 the Darcy permeability (square of the Brinkman screening length) of the gel. The permeability may be expressed as

$$\ell^2 = 1 / [n_s(r) 6\pi a_s F_s] = 2a_s^2 / (9\phi_s F_s), \quad (2.12)$$

where $n_s(r)$ is the concentration of Stokes resistance centers, with a_s and F_s the Stokes radius and drag coefficient of the polymer segments. In this work, n_s is constant, but,

[†] For convenience, the valence of the fixed charge is set opposite to that of its respective (mobile) counterion in Eqn. (2.4); this defines the concentration n_j^f .

in general, may vary with radial position r from the center of each inclusion. Note also that the Brinkman screening length is adjusted according to Eqn. (2.12) by varying the (uniform) polymer segment density with Stokes radius $a_s = 1 \text{ \AA}$. The drag coefficient F_s is obtained from an accurate correlation developed by Koch & Sangani (1999) for random fixed beds of spheres. In this work, however, only the reported values of ℓ are relevant. For example, the value $\ell \approx 0.951 \text{ nm}$, which is adopted for the principal set of tabulated results below, reflects a polymer segment concentration n_s that yields $\ell = 1 \text{ nm}$ according to Eqn. (2.12) when the Stokes radius $a_s = 1 \text{ \AA}$ and the drag coefficient $F_s = 1$. Because the hydrodynamic volume fraction $\phi = n_s(4/3)\pi a_s^3 > 0$, $F_s(\phi) > 1$ and, hence, ℓ is slightly less than the targeted value.

2.1.1. Inner (particle surface) boundary conditions

Either the equilibrium surface potential ζ or surface charge density σ may be specified. Because the surface ($r = a$) is assumed impenetrable with zero capacitance and conductance, the surface charge is constant, permitting no-flux boundary conditions for each (mobile) ion species. As usual, the no-slip boundary condition applies. It follows that (inner) boundary conditions are either

$$\psi = \zeta \text{ at } r = a \quad (2.13)$$

or

$$\epsilon_s \epsilon_o \nabla \psi|_{out} \cdot \hat{\mathbf{n}} - \epsilon_p \epsilon_o \nabla \psi|_{in} \cdot \hat{\mathbf{n}} = -\sigma \text{ at } r = a, \quad (2.14)$$

with

$$n_j \mathbf{v}_j \cdot \hat{\mathbf{n}} = 0 \text{ at } r = a \quad (2.15)$$

and

$$\mathbf{u} = \mathbf{0} \text{ at } r = a, \quad (2.16)$$

where $\hat{\mathbf{n}} = \mathbf{e}_r$ is an outward unit normal and ϵ_p is the particle dielectric constant.

2.1.2. Outer (far-field) boundary conditions

Neglecting particle interactions requires far-field boundary conditions

$$\psi \rightarrow -\mathbf{E} \cdot \mathbf{r} \text{ as } r \rightarrow \infty, \quad (2.17)$$

$$n_j \rightarrow n_j^\infty + \mathbf{B}_j \cdot \mathbf{r} \text{ as } r \rightarrow \infty, \quad (2.18)$$

and

$$\mathbf{u} \rightarrow \mathbf{U} \text{ as } r \rightarrow \infty, \quad (2.19)$$

where \mathbf{E} , \mathbf{B}_j and \mathbf{U} are, respectively, a constant electric field, constant species concentration gradients, and constant far-field velocity.

2.2. Solution of the equations

2.2.1. Equilibrium state

When $\mathbf{E} = \mathbf{B}_j = \mathbf{U} = \mathbf{0}$, equilibrium is specified according to

$$\epsilon_o \epsilon_s \nabla^2 \psi^0 = - \sum_{j=1}^N (n_j^0 - n_j^f) z_j e, \quad (2.20)$$

$$0 = \nabla \cdot [D_j \nabla n_j^0 + z_j e D_j / (kT) n_j^0 \nabla \psi^0] \quad (2.21)$$

and

$$0 = -\nabla p^0 - \sum_{j=1}^N n_j^0 z_j e \nabla \psi^0, \quad (2.22)$$

with boundary conditions

$$\psi^0 = \zeta \text{ at } r = a, \quad (2.23)$$

$$\epsilon_s \epsilon_o \nabla \psi^0|_{out} \cdot \mathbf{e}_r - \epsilon_p \epsilon_o \nabla \psi^0|_{in} \cdot \mathbf{e}_r = -\sigma \text{ at } r = a, \quad (2.24)$$

$$n_j^0 [D_j \nabla n_j^0 + z_j e D_j / (kT) n_j^0 \nabla \psi^0] \cdot \mathbf{e}_r = 0 \text{ at } r = a, \quad (2.25)$$

and

$$\psi^0 \rightarrow 0 \text{ as } r \rightarrow \infty, \quad (2.26)$$

$$n_j^0 \rightarrow n_j^\infty \text{ as } r \rightarrow \infty. \quad (2.27)$$

2.2.2. Linearized perturbed state

Perturbations to the equilibrium state (above) are introduced via

$$\psi = \psi^0 - \mathbf{E} \cdot \mathbf{r} + \psi', \quad (2.28)$$

$$n_j = n_j^0 + \mathbf{B}_j \cdot \mathbf{r} + n'_j, \quad (2.29)$$

and

$$p = p^0 + \mathbf{P} \cdot \mathbf{r} + p', \quad (2.30)$$

where the first terms on the right-hand sides denote the equilibrium values, with the primed quantities denoting perturbations. Note that \mathbf{P} is the far-field pressure gradient required to sustain a far-field velocity $\mathbf{U} = -(\ell^2/\eta)\mathbf{P}$.

With ‘forcing’

$$\mathbf{X} = X \mathbf{e}_z, \quad (2.31)$$

where $X \in \{E, B_j, U\}^\dagger$, the linearized perturbations are symmetric about the z -axis ($\theta = 0$) of a spherical polar coordinate system, taking the forms

$$\psi' = \hat{\psi}(r) \mathbf{X} \cdot \mathbf{e}_r \quad (2.32)$$

$$n'_j = \hat{n}_j(r) \mathbf{X} \cdot \mathbf{e}_r \quad (2.33)$$

and

$$\mathbf{u} = \mathbf{U} + \mathbf{u}', \quad (2.34)$$

where[‡]

$$\begin{aligned} \mathbf{u}' &= \nabla \times \nabla \times h(r) \mathbf{X} \\ &= -2(h_r/r)(\mathbf{X} \cdot \mathbf{e}_r) \mathbf{e}_r - (h_{rr} + h_r/r)(\mathbf{X} \cdot \mathbf{e}_\theta) \mathbf{e}_\theta. \end{aligned} \quad (2.35)$$

[†] In general, a linear combination of these variables.

[‡] Equation (2.35) guarantees a solenoidal (incompressible) velocity field, which permits the momentum equation to be solved by applying the curl $\nabla \times$, thereby eliminating the pressure and yielding a scalar equation for the single non-zero component of the vorticity $\nabla \times \mathbf{u} = \omega_\phi \mathbf{e}_\phi$.

The perturbations satisfy

$$\epsilon_o \epsilon_s \nabla^2 \psi' = - \sum_{j=1}^N (n'_j + \mathbf{B}_j \cdot \mathbf{r}) z_j e, \quad (2.36)$$

and

$$\nabla \cdot \mathbf{j}_j = 0, \quad (2.37)$$

where

$$\begin{aligned} \mathbf{j}_j = & -D_j(\nabla n'_j + \mathbf{B}_j) - z_j e D_j / (kT) (n'_j + \mathbf{B}_j \cdot \mathbf{r}) \nabla \psi^0 \\ & - z_j e D_j / (kT) n_j^0 (\nabla \psi' - \mathbf{E}) + n_j^0 (\mathbf{U} + \mathbf{u}'), \end{aligned} \quad (2.38)$$

and

$$\begin{aligned} \eta \nabla^2 \mathbf{u}' - \nabla p' - (\eta / \ell^2) (\mathbf{U} + \mathbf{u}') - \sum_{j=1}^N n_j^0 z_j e (\nabla \psi' - \mathbf{E}) \\ - \sum_{j=1}^N (n'_j + \mathbf{B}_j \cdot \mathbf{r}) z_j e \nabla \psi^0 = 0 \end{aligned} \quad (2.39)$$

$$\nabla \cdot \mathbf{u}' = 0, \quad (2.40)$$

with boundary conditions

$$\epsilon_s \epsilon_o (\nabla \psi' - \mathbf{E})|_{out} \cdot \mathbf{e}_r - \epsilon_p \epsilon_o (\nabla \psi' - \mathbf{E})|_{in} \cdot \mathbf{e}_r = 0 \text{ at } r = a, \quad (2.41)$$

$$\begin{aligned} n_j^0 [D_j(\nabla n'_j + \mathbf{B}_j \cdot \mathbf{r}) + z_j e D_j / (kT) (n'_j + \mathbf{B}_j \cdot \mathbf{r}) \nabla \psi^0 \\ + z_j e D_j / (kT) n_j^0 (\nabla \psi' - \mathbf{E}) - n_j^0 (\mathbf{U} + \mathbf{u}')] \cdot \mathbf{e}_r = 0 \text{ at } r = a, \end{aligned} \quad (2.42)$$

$$\mathbf{u}' = -\mathbf{U} \text{ at } r = a, \quad (2.43)$$

and

$$\psi' \rightarrow (\mathbf{X} \cdot \mathbf{e}_r) D^X / r^2 \text{ as } r \rightarrow \infty, \quad (2.44)$$

$$n'_j \rightarrow (\mathbf{X} \cdot \mathbf{e}_r) C_j^X / r^2 \text{ as } r \rightarrow \infty, \quad (2.45)$$

$$\mathbf{u}' \rightarrow -2(C^X / r^3)(\mathbf{X} \cdot \mathbf{e}_r) \mathbf{e}_r + (C^X / r^3)(\mathbf{X} \cdot \mathbf{e}_\theta) \mathbf{e}_\theta \text{ as } r \rightarrow \infty. \quad (2.46)$$

In the far field, the velocity disturbance \mathbf{u}' is proportional to the gradient of p' , which, like the electrostatic potential and ion concentrations, is dipolar. Accordingly, \mathbf{u}' decays as r^{-3} , and D^X and C_j^X will often be referred to as the strength of the electrostatic and concentration polarization (or dipole moments) induced by the field $X \in \{E, B_j, U\}$.

The dimensions of the *asymptotic coefficients* D^X , C_j^X and C^X , which depend on the respective $X \in \{E, B_j, U\}$, are easily worked out by inspecting Eqns. (2.44)–(2.46). For convenience, dimensionless values are presented in the tables below with a , $u^* = \epsilon_s \epsilon_o (kT/e)^2 / (\eta a)$, $2I$ and kT/e as the scales for length, velocity, ion concentrations, and electrostatic potential, respectively.

2.2.3. Superposition

The equations are solved using a numerical methodology developed by Hill *et al.* (2003) for the electrophoretic mobility of polymer-coated colloids. Solutions with E , B_j and U

set to arbitrary values can be computed, provided $\sum_{j=1}^N z_j B_j = 0$ to ensure an electrically neutral far-field. However, when N species are assembled into M electroneutral groups (*e.g.*, electrolytes or neutral tracers), each with far-field gradient B_k ($k = 1, \dots, M$), it is expedient to compute solutions with only one non-zero value of E , B_k or U . Then, arbitrary solutions can be obtained by linear superposition (O'Brien & White 1978).

An index k' is required to identify the (electroneutral) group to which the j th species under consideration is assigned. Careful consideration of the electrolyte composition and ion valences is required to ensure consistency. For z - z electrolytes, it is convenient to set $B_j = B_k$, whereas for a single 2-1 electrolyte (*e.g.*, CaCl_2), it is satisfactory to set $B_j = B_{k'}/|z_j|$. For the relatively simple situations considered in this work, the (single) electroneutral group is NaCl, so $M = 1$ with $k = k' = 1$, and $j = 1$ and 2 for Na^+ and Cl^- , respectively.

Note that $C_j^{B_k}$, for example, is the asymptotic coefficient for the perturbed *concentration* of the j th species induced by the k th concentration gradient B_k , whereas C^{B_k} (without a subscript) denotes the asymptotic coefficient for the *flow* induced by B_k .

For neutral species, the concentration disturbance produced by a single impenetrable sphere yields $C_j^{B_{k'}} = (1/2)a^3$, otherwise $C_j^{B_k} = 0$ ($k \neq k'$). Clearly, the asymptotic coefficients for charged species, whose concentration perturbations are influenced by electromigration, are not the same as for neutral species; for ions, $C_j^{B_{k'}} \rightarrow (1/2)a^3$ as $|\zeta| \rightarrow 0$, however.

With colinear forcing and bulk electroneutrality, linear superposition gives far-field decays

$$\psi' \rightarrow (1/r^2)[ED^E + \sum_{k=1}^M B_k D^{B_k} + UD^U](\mathbf{e}_z \cdot \mathbf{e}_r) \text{ as } r \rightarrow \infty, \quad (2.47)$$

$$n'_j \rightarrow (1/r^2)[EC_j^E + \sum_{k=1}^M B_k C_j^{B_k} + UC_j^U](\mathbf{e}_z \cdot \mathbf{e}_r) \text{ as } r \rightarrow \infty, \quad (2.48)$$

and

$$\begin{aligned} \mathbf{u}' &\rightarrow -(2/r^3)[EC^E + \sum_{k=1}^M B_k C^{B_k} + UC^U](\mathbf{e}_z \cdot \mathbf{e}_r)\mathbf{e}_r \\ &+ (1/r^3)[EC^E + \sum_{k=1}^M B_k C^{B_k} + UC^U](\mathbf{e}_z \cdot \mathbf{e}_\theta)\mathbf{e}_\theta \text{ as } r \rightarrow \infty. \end{aligned} \quad (2.49)$$

This work is *primarily* concerned with situations where only one $X \in \{E, B_j, U\}$ is applied. Following O'Brien & White (1978), these are referred to as the (E), (B) and (U) (microscale) problems. Algebraic or differential relationships between the averaged fields may be applied to ensure zero average current density, for example. The next section relates (microscale) \mathbf{E} , \mathbf{B}_j and \mathbf{U} to the averaged (macroscale) fields, *e.g.*, $-\langle \nabla \psi \rangle$, $\langle \nabla n_j \rangle$ and $\langle \mathbf{u} \rangle$, in *dilute* composites.

2.3. Averaged (bulk) fluxes

Here we calculate the average flux of the j th species

$$\langle \mathbf{j}_j \rangle = V^{-1} \int \mathbf{j}_j dV, \quad (2.50)$$

where the volume of integration includes the continuous and discrete phases. If the size of the *representative elementary volume* is between the micro- and macro-scales, the result

is equivalent to sampling the flux (at a point) over all micro-structural configurations (ensemble average).

Following Saville (1979) and O'Brien (1981), the averaging can be accomplished by adding and subtracting the flux

$$-D_j \nabla n_j - z_j e D_j / (kT) n_j^\infty \nabla \psi + n_j^\infty \mathbf{u} \quad (2.51)$$

from the integrand in Eqn. (2.50). This yields the macroscopic electromigrative, diffusive and convective fluxes in the absence of inclusions, plus an integral whose integrand is exponentially small beyond the diffuse double layers, *i.e.*,

$$\begin{aligned} \langle \mathbf{j}_j \rangle = & -z_j e D_j / (kT) n_j^\infty \langle \nabla \psi \rangle - D_j \langle \nabla n_j \rangle + n_j^\infty \langle \mathbf{u} \rangle \\ & + V^{-1} \int [z_j e D_j / (kT) n_j^\infty \nabla \psi + D_j \nabla n_j - n_j^\infty \mathbf{u} + \mathbf{j}_j] dV. \end{aligned} \quad (2.52)$$

Applying the divergence theorem[†] and noting that $\nabla \cdot \mathbf{j}_j = 0$, the volume integral in Eqn. (2.52) becomes

$$\begin{aligned} & \int z_j e D_j / (kT) n_j^\infty \psi \hat{\mathbf{n}} dA - \int z_j e D_j / (kT) n_j [\nabla \psi \cdot \hat{\mathbf{n}}] \mathbf{r} dA \\ & + \int D_j n_j \hat{\mathbf{n}} dA - \int D_j [\nabla n_j \cdot \hat{\mathbf{n}}] \mathbf{r} dA \\ & + \int (n_j - n_j^\infty) (\mathbf{u} \cdot \hat{\mathbf{n}}) \mathbf{r} dA, \end{aligned} \quad (2.53)$$

where the integrals enclose the inclusions and their respective equilibrium double layer, with $\hat{\mathbf{n}}$ directed outward, into the fluid.

For dilute composites, *i.e.*, when $n(4/3)\pi(a + \kappa^{-1})^3 \ll 1$, the integral over a representative volume V equals nV integrals with a single particle at $\mathbf{r} = \mathbf{0}$, each with $\hat{\mathbf{n}} = \mathbf{e}_r$. Therefore, noting that $n_j^0 - n_j^\infty$ is exponentially small as $r \rightarrow \infty$, and that n'_j and $\mathbf{B}_j \cdot \mathbf{r}$ are odd functions of position, the fluxes become

$$\begin{aligned} \langle \mathbf{j}_j \rangle \approx & n_j^\infty \langle \mathbf{u} \rangle - z_j e D_j / (kT) n_j^\infty \langle \nabla \psi \rangle - D_j \langle \nabla n_j \rangle \\ & + n z_j e D_j / (kT) n_j^\infty \int_{r \rightarrow \infty} [\psi' - (\nabla \psi' \cdot \mathbf{r})] \mathbf{e}_r dA \\ & + n D_j \int_{r \rightarrow \infty} [n'_j - (\nabla n'_j \cdot \mathbf{r})] \mathbf{e}_r dA. \end{aligned} \quad (2.54)$$

Superposing solutions of the independent single-particle problems, the microscale electromigrative and diffusive contributions to the average flux, *i.e.*, the last two terms in Eqn. (2.54), are, respectively[‡],

$$\begin{aligned} & n z_j e D_j / (kT) n_j^\infty \int_{r \rightarrow \infty} [\psi' - (\nabla \psi' \cdot \mathbf{r})] \mathbf{e}_r dA = \\ & n 4\pi z_j e D_j / (kT) n_j^\infty [\mathbf{E} D^E + \sum_{k=1}^M \mathbf{B}_k D^{B_k} + \mathbf{U} D^U], \end{aligned} \quad (2.55)$$

[†] Note also that $\int_V \boldsymbol{\alpha} dV = \int_A \mathbf{x} \boldsymbol{\alpha} \cdot \hat{\mathbf{n}} dA - \int_V \mathbf{x} \nabla \cdot \boldsymbol{\alpha} dV$, where $\boldsymbol{\alpha}$ represents an arbitrary vector field.

[‡] Note, $\mathbf{r}(\boldsymbol{\alpha} \cdot \mathbf{e}_r)$ has been written as $(\boldsymbol{\alpha} \cdot \mathbf{r}) \mathbf{e}_r$ because $\mathbf{r} = r \mathbf{e}_r$, where $\boldsymbol{\alpha}$ represents an arbitrary vector field.

and

$$nD_j \int_{r \rightarrow \infty} [n'_j - (\nabla n'_j \cdot \mathbf{r})] \mathbf{e}_r dA = n4\pi D_j [\mathbf{E}C_j^E + \sum_{k=1}^M \mathbf{B}_k C_j^{B_k} + \mathbf{U}C_j^U]. \quad (2.56)$$

Substituting these into Eqn. (2.54) gives

$$\begin{aligned} \langle \mathbf{j}_j \rangle &\approx n_j^\infty \langle \mathbf{u} \rangle - z_j e D_j / (kT) n_j^\infty \langle \nabla \psi \rangle - D_j \langle \nabla n_j \rangle \\ &+ n4\pi z_j e D_j / (kT) n_j^\infty [\mathbf{E}D^E + \sum_{k=1}^M \mathbf{B}_k D^{B_k} + \mathbf{U}D^U] \\ &+ n4\pi D_j [\mathbf{E}C_j^E + \sum_{k=1}^M \mathbf{B}_k C_j^{B_k} + \mathbf{U}C_j^U]. \end{aligned} \quad (2.57)$$

Note that the average fluxes are now expressed in terms of the asymptotic coefficients from at most $2+M$ independent single-particle problems, each of which is solved ‘exactly’ in this work.

2.4. Averaged (bulk) momentum conservation equations

In general, an average velocity $\langle \mathbf{u} \rangle$ is produced by the application of an average pressure gradient $\langle \nabla p \rangle$, electric field $-\langle \nabla \psi \rangle$, or concentration gradients $\langle \nabla n_j \rangle$. Here we link these to the asymptotic coefficients from the single-particle problem. Accordingly, averaging the momentum equation and neglecting products of perturbed quantities gives

$$\mathbf{0} = -\langle \nabla p' \rangle - (\eta/\ell^2) \langle \mathbf{u} \rangle + \eta \nabla^2 \langle \mathbf{u} \rangle - n \langle \mathbf{f} \rangle - \langle \rho^0 \nabla \psi' \rangle - \langle \rho' \nabla \psi^0 \rangle, \quad (2.58)$$

where $\rho = \rho^0 + \rho'$ is the charge density, $\nabla p = \nabla p^0 + \langle \nabla p \rangle + \nabla p'$, and $\langle \mathbf{f} \rangle$ is the average (hydrodynamic) force exerted by the fluid on the inclusions. Note that the electrical force on the inclusions is transmitted to the polymer gel, which, in turn, is balanced by the Darcy drag force exerted by the fluid on the (assumed rigid) polymer. Furthermore, spatial and temporal acceleration is neglected, and Eqn. (2.58) neglects contributions to the stress from hydrodynamic and electrostatic interactions, so the analysis is limited to small volume fractions $n(4/3)\pi(a + \kappa^{-1})^3 \ll 1$.

Similarly to the average fluxes, let us adopt the single-particle problem to evaluate the average body force $\langle \mathbf{f} \rangle$. For a *single* inclusion in an *unbounded* polymer gel, the hydrodynamic force is

$$\begin{aligned} \langle \mathbf{f} \rangle &\approx \int_{r=a} [-(\mathbf{P} \cdot \mathbf{r} + p')\delta + 2\eta \mathbf{e}] \cdot \mathbf{e}_r dA \\ &= \int_{r \rightarrow \infty} [-(\mathbf{P} \cdot \mathbf{r} + p')\delta + 2\eta \mathbf{e}] \cdot \mathbf{e}_r dA \\ &\quad - \int_{r=a}^\infty [(\eta/\ell^2)\mathbf{u} + \rho^0 \nabla \psi' + \rho' \nabla \psi^0] dV, \end{aligned} \quad (2.59)$$

where $\mathbf{e} = (1/2)[\nabla \mathbf{u} + (\nabla \mathbf{u})^T]$ and δ is the identify tensor. Since $\nabla \cdot \mathbf{u} = 0$, $\mathbf{u}(r=a) = \mathbf{0}$, $\mathbf{P} = -(\eta/\ell^2)\mathbf{U}$, and $\mathbf{u}' \sim r^{-3}$ as $r \rightarrow \infty$, Eqn. (2.59) becomes

$$\langle \mathbf{f} \rangle \approx - \int_{r \rightarrow \infty} [p' + (\eta/\ell^2)(\mathbf{u}' \cdot \mathbf{r})] \mathbf{e}_r dA - \int_{r=a}^\infty (\rho^0 \nabla \psi' + \rho' \nabla \psi^0) dV. \quad (2.60)$$

Beyond the double layer,

$$p' = -(\eta/\ell^2) \int_r^\infty (2/r'^3) C^X(\mathbf{X} \cdot \mathbf{e}_r) dr' = -(1/r^2)(\eta/\ell^2) C^X(\mathbf{X} \cdot \mathbf{e}_r) \quad (2.61)$$

and, because the integrand of the volume integral in Eqn. (2.60) is exponentially small there (for a single sphere in an unbounded polymer gel),

$$n \int_{r=a}^{\infty} (\rho^0 \nabla \psi' + \rho' \nabla \psi^0) dV = \langle \rho^0 \nabla \psi' \rangle + \langle \rho' \nabla \psi^0 \rangle. \quad (2.62)$$

Therefore,

$$\langle \mathbf{f} \rangle \approx (\eta/\ell^2) 4\pi [\mathbf{E} C^E + \sum_{k=1}^M \mathbf{B}_k C^{B_k} + \mathbf{U} C^U] - n^{-1} \langle \rho^0 \nabla \psi' \rangle - n^{-1} \langle \rho' \nabla \psi^0 \rangle, \quad (2.63)$$

and, finally, Eqn. (2.58) becomes

$$\langle \nabla p \rangle \approx -(\eta/\ell^2) \langle \mathbf{u} \rangle + \eta \nabla^2 \langle \mathbf{u} \rangle - n(\eta/\ell^2) 4\pi [\mathbf{E} C^E + \sum_{k=1}^M \mathbf{B}_k C^{B_k} + \mathbf{U} C^U]. \quad (2.64)$$

2.5. Averaged (bulk) equations for unidirectional transport

With *all* average fluxes in the z -direction, mass and momentum conservation require constant $\langle \mathbf{u} \rangle$ and, hence,

$$\langle \nabla p \rangle = -(\eta/\ell^2) \langle \mathbf{u} \rangle - \phi(3/a^3)(\eta/\ell^2) [\mathbf{E} C^E + \sum_{k=1}^M \mathbf{B}_k C^{B_k} + \mathbf{U} C^U]. \quad (2.65)$$

Similarly, the (steady) average species conservation equations $\nabla \cdot \langle \mathbf{j}_j \rangle = 0$ require constant average fluxes

$$\begin{aligned} \langle \mathbf{j}_j \rangle &= n_j^\infty \langle \mathbf{u} \rangle - z_j e D_j / (kT) n_j^\infty \langle \nabla \psi \rangle - D_j \langle \nabla n_j \rangle \\ &+ \phi(3/a^3) z_j e D_j / (kT) n_j^\infty [\mathbf{E} D^E + \sum_{k=1}^M \mathbf{B}_k D^{B_k} + \mathbf{U} D^U] \\ &+ \phi(3/a^3) D_j [\mathbf{E} C_j^E + \sum_{k=1}^M \mathbf{B}_k C_j^{B_k} + \mathbf{U} C_j^U]. \end{aligned} \quad (2.66)$$

Note that $\nabla \cdot \langle \nabla \psi \rangle = 0$ in an electrically neutral composite with uniform dielectric permittivity, so the average electric field is also constant.

The averages can be expanded as a power series in the inclusion volume fraction *e.g.*, $\langle \mathbf{u} \rangle \rightarrow \mathbf{U}_0 + \phi \mathbf{U}_1 + O(\phi^2)$. Therefore, since the microscale equations (asymptotic coefficients) are accurate to $O(\phi)$, the notation is condensed by writing, for example, $\langle \mathbf{u} \rangle \equiv \mathbf{U}$, where it is understood that $\mathbf{U} = \mathbf{U}_0 + \phi \mathbf{U}_1 + O(\phi^2)$. Clearly, \mathbf{E} , \mathbf{B}_j , and \mathbf{U} in Eqns. (2.65) and (2.66) need only include the $O(1)$ contribution to their respective average, *e.g.*, $\mathbf{U} \rightarrow \mathbf{U}_0$. The following notation is adopted for the other averaged quantities: $\mathbf{J}_j \equiv \langle \mathbf{j}_j \rangle$, $\mathbf{P} \equiv \langle \nabla p \rangle$, $\mathbf{B}_j \equiv \langle \nabla n_j \rangle$, $\mathbf{E} \equiv -\langle \nabla \psi \rangle$.

With one electrolyte ($M = 1$) and, recall, bulk electroneutrality, there are $N + 4$ independent variables ($\mathbf{E}, \mathbf{U}, \mathbf{P}, \mathbf{B}_k$ ($k = 1$), \mathbf{J}_j ($j = 1, \dots, N$)) with $N + 1$ independent equations (Eqns. (2.65) and (2.66)). Clearly, three independent variables must be specified for a unique solution. For clarity, the results presented below involve a 1-1 electrolyte (NaCl), mostly with only one non-zero forcing variable. It is important to note that, because the equations are linear, solutions for any combination of forcing variables may be constructed. For example, an accompanying paper establishes the electric field strength required to maintain a constant electrolyte flux—driven by a bulk concentration gradient across a membrane—with zero bulk current density.

3. Response to an electric field

Results are now presented for the application of an electric field in the absence of average pressure and concentration gradients. These conditions prevail when measuring the electrical conductivity, for example, and they provide a relatively simple setting in which to study the influence of inclusions on bulk electrokinetic transport. Steady homogeneous conditions are assumed, neglecting the influence of electrode polarization and electrochemical reactions. Accordingly, the average velocity from Eqn. (2.65) is

$$\mathbf{U} = -\phi(3/a^3)\mathbf{E}C^E + O(\phi^2), \quad (3.1)$$

and the average ion fluxes from Eqn. (2.66) are

$$\begin{aligned} \mathbf{J}_j = & z_j e D_j / (kT) n_j^\infty \mathbf{E} + \phi(3/a^3) z_j e D_j / (kT) n_j^\infty \mathbf{E} D^E \\ & + \phi(3/a^3) D_j \mathbf{E} C_j^E + \phi(3/a^3) n_j^\infty \mathbf{E} C^E + O(\phi^2). \end{aligned} \quad (3.2)$$

Asymptotic coefficients are listed in table 1 for a composite with Brinkman screening length $\ell \approx 0.951$ nm and inclusion radius $a = 100$ nm; the ζ -potentials and (three) ionic strengths span experimentally accessible ranges. With a positive electric field ($E > 0$), the counterions (Na^+) migrate toward the ‘front’ of the inclusions, inducing a positive electrostatic dipole moment $D^E > 0$. When the ζ -potential is low, however, the dipole moment reflects the dielectric polarization required to maintain an impenetrable interface, so the dipole strength approaches the Maxwell value $D^E = -(1/2)a^3$ (for non-conducting spheres) as $|\zeta| \rightarrow 0$. The positive concentration dipole moments $C_j^E > 0$ reflect the combined influences of electromigration, diffusion, and electroneutrality. As expected from Eqn. (2.46), $C^E < 0$, because the electrical force on the fluid and, hence, the resulting electroosmotic flow are forward ($U > 0$).

3.1. Incremental pore velocity

As suggested by Eqn. (3.1), the ratio

$$U/(E\phi) = -3C^E/a^3, \quad (3.3)$$

which is termed the *incremental pore mobility*, provides a convenient measure of the electroosmotic pumping capacity. When multiplied by the electric field strength and particle volume fraction, the values listed in the last column of table 1, for example, yield the $O(\phi)$ average velocity that prevails in the absence of an applied pressure gradient. This section examines how the strength of the flow is related to the ζ -potential and size of the inclusions, the ionic strength, and permeability of the gel. We will see that the pore mobility is significantly influenced by polarization and relaxation, so the qualitative form of the relationship (with a given gel permeability) is similar to the classical electrophoretic mobility of dispersions (O’Brien & White 1978).

Consider the case in table 1 with $\kappa a = 100$ and $\zeta = -1kT/e$. With $E = 2$ V cm⁻¹ and $\phi = 10^{-2}$, the pore velocity is $U \approx 0.84$ nm s⁻¹, which is clearly very slow. If, however, this flow is directed from a composite with a 1 cm² cross-section into a microfluidic channel, then it is not unreasonable to amplify the velocity by four orders of magnitude, yielding a (modest) average velocity of 8.4 μ m s⁻¹. In this example, the permeability ($\ell^2 = 0.951^2$ nm²) is relatively low, so higher velocities may be achieved with a comparable (weak) electric field and inclusion volume fraction. Note that a stronger electric field between (platinum) electrodes separated by a distance $L \sim 5$ mm, say, produces hydrogen and oxygen bubbles. In ‘conventional’ electroosmotic pumps, much higher electric field strengths are achieved by catalytically recombining hydrogen and

TABLE 1. Scaled (dimensionless) asymptotic coefficients (see Eqn. (3.2)) and *incremental pore mobility* (Eqn. (3.1)) for bulk *electromigration* of NaCl in a Brinkman medium with charged spherical inclusions: $a = 100$ nm; $\ell \approx 0.951$ nm; $T = 25^\circ\text{C}$; $D_1 \approx 1.33 \times 10^{-9} \text{m}^2 \text{s}^{-1}$ (Na^+); $D_2 \approx 2.03 \times 10^{-9} \text{m}^2 \text{s}^{-1}$ (Cl^-); $u^* = \epsilon_s \epsilon_o (kT/e)^2 / (\eta a) \approx 5.15 \times 10^{-3} \text{m s}^{-1}$.

$\zeta e / (kT)$	D^E / a^3	$C_j^E kT / (2I a^3 e)$ ($j = 1, 2$)	$C^E kT / (u^* a^4 e)$	$U / (E\phi) = -3C^E / a^3$ ((nm s ⁻¹)/(V cm ⁻¹))
<hr/>				
$\kappa a = 1$	$I = 9.25 \times 10^{-6} \text{mol l}^{-1}$			
<hr/>				
-1	-3.82×10^{-1}	1.04×10^0	-1.87×10^{-4}	1.13×10^0
-2	-5.71×10^{-2}	2.04×10^0	-3.66×10^{-4}	2.20×10^0
-4	$+8.66 \times 10^{-1}$	3.72×10^0	-6.64×10^{-4}	3.99×10^0
-6	$+1.60 \times 10^0$	4.77×10^0	-8.40×10^{-4}	5.05×10^0
-8	$+1.96 \times 10^0$	5.28×10^0	-9.04×10^{-4}	5.44×10^0
<hr/>				
$\kappa a = 10$	$I = 9.25 \times 10^{-4} \text{mol l}^{-1}$			
<hr/>				
-1	-4.74×10^{-1}	7.30×10^{-2}	-1.20×10^{-3}	7.22×10^0
-2	-3.98×10^{-1}	1.51×10^{-1}	-2.42×10^{-3}	1.46×10^1
-4	-1.37×10^{-1}	3.24×10^{-1}	-4.63×10^{-3}	2.78×10^1
-6	$+1.32 \times 10^{-1}$	4.76×10^{-1}	-5.45×10^{-3}	3.28×10^1
-8	$+2.95 \times 10^{-1}$	5.64×10^{-1}	-4.70×10^{-3}	2.83×10^1
<hr/>				
$\kappa a = 100$	$I = 9.25 \times 10^{-2} \text{mol l}^{-1}$			
<hr/>				
-1	-4.96×10^{-1}	7.83×10^{-3}	-6.97×10^{-3}	4.19×10^1
-2	-4.82×10^{-1}	1.79×10^{-2}	-1.42×10^{-2}	8.51×10^1
-4	-4.11×10^{-1}	5.58×10^{-2}	-2.87×10^{-2}	1.73×10^2
-6	-2.53×10^{-1}	1.35×10^{-1}	-3.83×10^{-2}	2.30×10^2
-8	-3.81×10^{-2}	2.43×10^{-1}	-3.58×10^{-2}	2.15×10^2
<hr/>				

oxygen (Yao *et al.* 2003). For the purpose of accurately ‘measuring’ the pore mobility, however, higher electric field strengths are, perhaps, unnecessary.

The pore mobility is shown in the *left panels* of figure 3 as a function of the ζ -potential for various values of κa , with particle radii $a = 10, 100$ and 1000 nm (*top-to-bottom panels*), and Brinkman screening length $\ell \approx 3.11$ nm. The relationship is similar to the classical electrophoretic mobility (*e.g.*, O’Brien & White 1978), providing a one-to-one connection between the (measured) pore velocity and the surface charge at low to moderate ζ -potentials. Mobility maxima arise from polarization (by electromigration) and relaxation (by diffusion) of the equilibrium double layer. As suggested by earlier theoretical studies examining the role of polarization and relaxation on the electrophoretic mobility of polymer-coated particles (Saville 2000; Hill 2004; Hill & Saville 2005), these calculations clearly demonstrate that polarization is driven by electromigration, since convection is extremely weak when the particles are immobilized in a polymer gel. Note that theoretical studies of electroosmotic flow in micro-porous membranes do not reveal such maxima, because the underlying microscale model comprises (effectively) straight channels with charged walls (Yao & Santiago 2003).

As expected, the (incremental) pore mobility tends to increase with ζ -potential at fixed ionic strength, and increases with ionic strength at fixed ζ -potential. Both trends reflect the increasing charge required to maintain a constant surface potential when varying the ionic strength. For colloids whose surface charge is independent of electrolyte concentration, the ζ -potential increases with decreasing κa . Accurate semi-empirical expressions for this relationship (obtained from solutions of the Poisson-Boltzmann equation) are readily available (Russel *et al.* 1989). In general, however, the dependence of surface charge density on ionic strength and pH is exceedingly difficult to predict, and must therefore be determined empirically for specific interfaces (*e.g.*, see Yao *et al.* 2003, for silica in the presence of KCl).

To draw a closer connection to experiments, the pore mobility is shown in the *right panels* of figure 3 as a function of the ionic strength with three *constant* surface charge densities, spanning two orders of magnitude. Note that the inclusion radii are the same as in the corresponding *left panels*. Because the surface charge is fixed, the ζ -potential (*dashed lines*, right axis) decreases with increasing ionic strength, but the particle size does not significantly influence the ζ -potential. Because the average velocity reflects the combined influence of all particles in the composite, U is expected to be proportional to the $O(n\sigma a^2 \sim \sigma\phi/a)$ (average) counter-charge density. Therefore, balancing the corresponding $O(E\phi/a)$ electrical force with an $O(\eta U/\ell^2)$ Darcy drag force gives a pore mobility $U/(\phi E) \sim \sigma\ell^2/a$. Indeed, comparing the mobility axes (left sides) of the panels on the right-hand side of figure 3 indicates that the mobility is, at least approximately, inversely proportional to the inclusion radius. Again, at low ionic strengths, when the ζ -potential is large, polarization and relaxation significantly complicate this simple interpretation.

To highlight the influence of polymer-gel permeability, the pore mobility is shown in figure 4 as a function of the Brinkman screening length ℓ for various ζ -potentials. With a particle radius $a = 100$ nm, the ionic strength $I \approx 0.0925$ mol l⁻¹ yields $\kappa a = 100$ and $\kappa\ell > 1$ at most values of ℓ . Now the mobility increases as ℓ^m with $m(\ell)$ in the range 1–2, indicating that viscous stresses *and* Darcy drag balance the electrical body force. Note that the mobility increases linearly with the ζ -potential when $|\zeta|$ is small, and, again, mobility maxima are evident when $|\zeta| \approx 6kT/e$. Pore mobilities are shown in figure 5 at a much lower ionic strength $I \approx 9.25 \times 10^{-6}$ mol l⁻¹ yielding $\kappa a = 1$. Now, as expected, the mobility increases linearly with ℓ^2 , since $\kappa\ell < 1$. Note that the monotonic increase

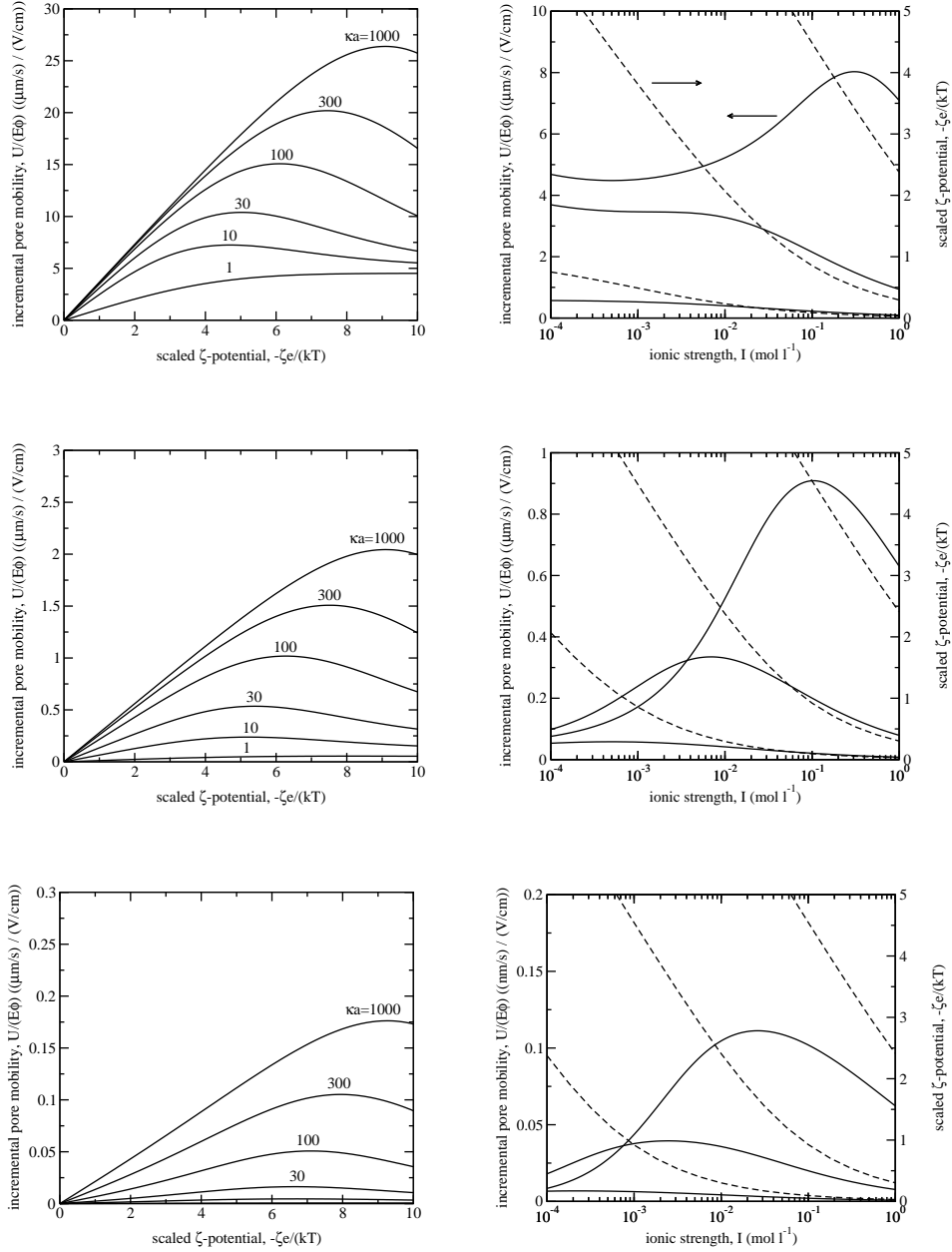


FIGURE 3. The incremental pore mobility $U/(E\phi)$ with inclusion radii $a = 10$ (top), 100 (middle) and 1000 nm (bottom): aqueous NaCl at $T = 25^\circ\text{C}$; $\ell \approx 3.11$ nm. Left panels show the mobility as a function of the (scaled) ζ -potential $\zeta_e/(kT)$ for various (scaled) reciprocal double-layer thicknesses $\kappa a = 1, 10, 30, 100, 300$ and 1000. Right panels shows the mobility (solid lines, left axis) and ζ -potential (dashed lines, right axis) as a function of the ionic strength with constant surface charge densities $\sigma \approx 0.179, 1.79$ and $17.9 \mu\text{C cm}^{-2}$ (increasing upward).

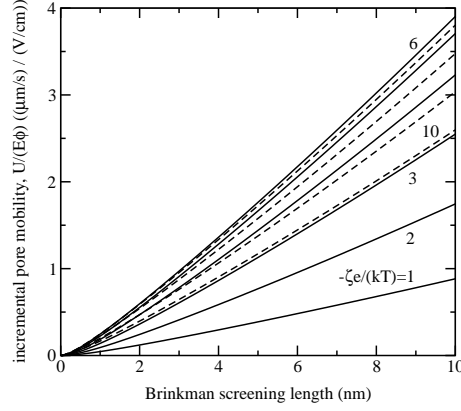


FIGURE 4. The incremental pore mobility $U/(E\phi)$ as a function of the Brinkman screening length ℓ for various (scaled) ζ -potentials $-\zeta e/(kT) = 1, 2, 3, \dots, 6$ (*solid lines*) $7, \dots, 10$ (*dashed lines*): aqueous NaCl at $T = 25^\circ\text{C}$; $a = 100$ nm; $\kappa a = 100$ ($I \approx 0.0925$ mol l^{-1}). An electric field is applied in the absence of average pressure and concentration gradients. The maximum velocity is achieved when $|\zeta|e/(kT) \approx 6$.

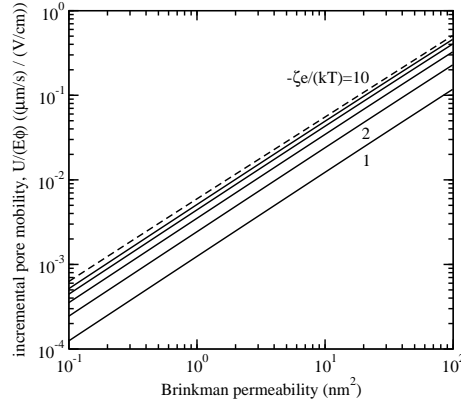


FIGURE 5. The incremental pore mobility $U/(E\phi)$ as a function of the Darcy permeability ℓ^2 for various (scaled) ζ -potentials $-\zeta e/(kT) = 1, 2, 3, \dots, 6$ (*solid lines*) 10 (*dashed line*): aqueous NaCl at $T = 25^\circ\text{C}$; $a = 100$ nm; $\kappa a = 1$ ($I \approx 9.25 \times 10^{-6}$ mol l^{-1}).

with ζ -potential is because the surface charge densities are low and, hence, polarization is weak.

3.2. Electroosmotic pumping

Recall, the (incremental) pore mobility was defined with zero average pressure gradient, and therefore neglects the pressure differential $\Delta p = PL$ required to pump fluid through an external network. This section briefly addresses coupling of the composite and electrodes—which together are referred to as an electroosmotic pump—to a mi-

crofluidic network. The analysis briefly considers the force exerted on the composite, the electrical power consumption, and pump efficiency.

Let us consider a closed loop, where fluid in the composite exits from one side, passes through a microfluidic network, and returns to the other side. To ensure that all electrical current flows through the composite, we assume that the electrical resistance of the network is much greater than of the pump, which is realized when the length (area) of the external network L_e (d^2) is much greater (smaller) than that of the composite L (A). Next, assuming laminar viscous flow, the pressure-drop through the network may be written

$$\Delta p \approx \eta c(L_e/d^4)Q, \quad (3.4)$$

where d^2 is the (characteristic) channel cross-sectional area, Q is the volumetric flow rate, and c is an $O(1)$ constant that reflects the shape and length the network sections.

Equating the network pressure drop to the “pump characteristic” emerging from Eqn. (2.64),

$$\Delta p/L = -(\eta/\ell^2)U - \phi(3/a^3)(\eta/\ell^2)(EC^E + UC^U), \quad (3.5)$$

gives

$$[\eta c(L_e/d^4)(A/L) + (\eta/\ell^2) + \phi(3/a^3)(\eta/\ell^2)C^U](Q/A) = -\phi(3/a^3)(\eta/\ell^2)EC^E, \quad (3.6)$$

where A and L are, respectively, the composite cross-sectional area and length.

The contribution of the back-flow, as represented by the asymptotic coefficient C^U in Eqn. (3.6), is obtained from the (U) problem. This and other asymptotic coefficients are listed in table 2 for a composite with Brinkman screening length $\ell \approx 0.951$ nm and inclusion radius $a = 100$ nm; again, the ζ -potentials and (three) ionic strengths span experimentally accessible ranges. Clearly, the drag force on the inclusions $\mathbf{f} = (\eta/\ell^2)4\pi C^U \mathbf{U}$ (see Eqn. (2.63)) is independent of the surface charge. Note that $C^U = (1/2)a^3$ when the only contribution to the drag force is due to Darcy flow ($\ell/a \ll 1$). Therefore, the (constant) value $C^U/a^3 \approx 0.514$ in table 2 ($\ell/a \sim 0.01$) reflects a small viscous contribution. The flow-induced electrical and concentration polarization, as represented by D^U and C_j^U , are related to the so-called streaming potential and streaming current, and are included here only for future reference.

When the dominant resistance comes from the composite itself (the second term on the left-hand-side of Eqn. (3.6)), the “pump performance curve” simplifies to

$$Q \approx -\phi(3/a^3)AEC^E, \quad (3.7)$$

which is clearly independent of the applied load. Neglecting constraints imposed by electrolysis, for example, the maximum length of the composite may be set by consideration of the electrical power consumption

$$\mathcal{P} \approx K^\infty E^2 AL + O(\phi). \quad (3.8)$$

Note that the force exerted on the composite

$$F = -\Delta p A \approx \eta c(L_e/d^4)A^2 \phi(3/a^3)EC^E \quad (3.9)$$

reflects the pressure required to pump fluid through the network. Therefore, the average shear stress $\tau \sim -F/(L\sqrt{A})$ required to support the composite scales as

$$\tau \sim -\eta c(L_e/d^4)(A^{3/2}/L)\phi(3/a^3)EC^E. \quad (3.10)$$

Since A will be set by the flow rate, the length of the composite must be set by the maximum allowable shear stress.

TABLE 2. Asymptotic coefficients for average *convection* of NaCl in a Brinkman medium with charged spherical inclusions: $a = 100$ nm; $\ell = 0.951$ nm; $T = 25^\circ\text{C}$, $D_1 \approx 1.33 \times 10^{-9} \text{m}^2 \text{s}^{-1}$ (Na^+); $D_2 \approx 2.03 \times 10^{-9} \text{m}^2 \text{s}^{-1}$ (Cl^-); $u^* \approx 5.15 \times 10^{-3} \text{ m s}^{-1}$.

$\zeta e/(kT)$	$D^U e u^*/(kT a^2)$	$C_j^U u^*/(2I a^2)$ ($j = 1, 2$)	C^U/a^3
$\kappa a = 1$	$I = 9.25 \times 10^{-6} \text{ mol l}^{-1}$		
-1	6.70×10^{-1}	8.71×10^{-2}	5.14×10^{-1}
-2	1.32×10^0	2.03×10^{-1}	5.14×10^{-1}
-4	2.44×10^0	4.49×10^{-1}	5.14×10^{-1}
-6	3.10×10^0	6.06×10^{-1}	5.14×10^{-1}
-8	3.33×10^0	6.44×10^{-1}	5.14×10^{-1}
$\kappa a = 10$	$I = 9.25 \times 10^{-4} \text{ mol l}^{-1}$		
-1	4.38×10^{-2}	7.76×10^{-4}	5.14×10^{-1}
-2	9.10×10^{-2}	2.16×10^{-3}	5.14×10^{-1}
-4	1.81×10^{-1}	5.58×10^{-3}	5.14×10^{-1}
-6	2.19×10^{-1}	7.08×10^{-3}	5.14×10^{-1}
-8	1.96×10^{-1}	5.74×10^{-3}	5.14×10^{-1}
$\kappa a = 100$	$I = 9.25 \times 10^{-2} \text{ mol l}^{-1}$		
-1	2.55×10^{-3}	4.49×10^{-6}	5.14×10^{-1}
-2	5.33×10^{-3}	1.27×10^{-5}	5.14×10^{-1}
-4	1.14×10^{-2}	3.69×10^{-5}	5.14×10^{-1}
-6	1.64×10^{-2}	5.93×10^{-5}	5.14×10^{-1}
-8	1.70×10^{-2}	6.14×10^{-5}	5.14×10^{-1}

Transport in polymer-gel composites

Finally, the pump efficiency, as measured by the ratio of the rate of flow work $|Q\Delta p|$ to the electrical power consumption \mathcal{P} is

$$\mathcal{E} \approx \eta c(L_e/d^4)[\phi(3/a^3)C^E]^2 A/(K^\infty L). \quad (3.11)$$

Because C^E depends on ζ , κa , ℓ , etc., care must be taken in interpreting this equation. Nevertheless, geometrical considerations alone clearly favor thin membranes with large cross-sectional area, operating with a low ionic strength (conductivity) and a high inclusion volume fraction. In practice, an optimal design (with specified flow Q and, perhaps, voltage $V = \Delta\psi$) will be constrained by consideration of the mechanical strength of the composite (as indicated by Eqns. (3.9) and (3.10)), which clearly diminishes with decreasing thickness L and increasing area A .

3.3. Incremental pressure gradient

Now consider the pressure gradient produced by an average electric field with zero average flow. This situation may be realized when an electrolyte-saturated composite is bounded by a vessel with impenetrable walls. A practical application involves measuring the differential (static) pressure Δp to infer the permeability of the polymer gel or, for example, the ζ -potential of the inclusions. Note that zero average flow does not imply stationary fluid at the microscale, because the ‘inner’ electroosmotic flow around each inclusion is balanced by a far-field pressure-driven back-flow, analogous to the situation encountered in microelectrophoresis capillaries with blocked ends.

Setting $U = 0$ in Eqn. (2.65) gives

$$\mathbf{P} = -\phi(\eta/\ell^2)(3/a^3)C^E \mathbf{E} + O(\phi^2), \quad (3.12)$$

which is termed the *incremental pressure gradient*. Representative values may be calculated by multiplying the incremental pore mobilities in the last column of table 1, and plotted in figures 3–5, by their respective values of η/ℓ^2 .

It is interesting to note that when $\kappa\ell < 1$ and, hence, the pore mobility increases linearly with ℓ^2 (see figure 5), the pressure gradient is independent of the permeability. This is because increasing the permeability increases the electric-field-induced flow, and, since the back-flow and accompanying pressure gradient are proportional to each other, it follows that the pressure gradient is independent of ℓ^2 . However, at higher ionic strengths, when $\kappa\ell > 1$ (see figure 4), the pressure gradient evidently decreases with ℓ^2 . This is because the electric-field-induced flow within the diffuse double layers—where resistance to flow is predominantly due to viscous stress—increases more slowly with the permeability than the Darcy drag beyond the double layers decreases.

Note that the incremental pressure gradient reflects the same asymptotic coefficient C^E as the pore mobility, so it is important to establish whether measuring the electric-field-induced pressure gradient offers a significant advantage over measuring the pore mobility. Recall, pore mobilities can generate low but measurable velocities in a microchannel. From table 1 with $\kappa a = 100$ and $\zeta = -1kT/e$, setting $E = 2 \text{ V cm}^{-1}$ and $\phi = 10^{-2}$ yields $P \approx 8.76 \text{ kPa cm}^{-1}$. Therefore, when $L = 5 \text{ mm}$, for example, the pressure differential is $|\Delta p| \approx 4.38 \text{ kPa}$ (static head of 0.43 m of water). Clearly, the pressure gradient induced by a relatively weak electric field is sufficient to produce a modest (static) pressure.

3.4. Species fluxes

Let us write the average flux of each species from Eqn. (3.2) as

$$\mathbf{J}_j = z_j e D_j / (kT) n_j^\infty \mathbf{E} (1 + \phi \Delta_j^E), \quad (3.13)$$

where

$$\begin{aligned}\Delta_j^E &= \Delta_{j,e}^E + \Delta_{j,d}^E + \Delta_{j,c}^E \\ &= (3/a^3)D^E + (3/a^3)kT/(z_j e n_j^\infty)C_j^E + (3/a^3)kT/(z_j e D_j)C^E\end{aligned}\quad (3.14)$$

is the sum of incremental *microscale* contributions (of electromigration, diffusion, and convection, respectively) to the average electromigrative flux.

The ratio of the convective and electromigrative terms is

$$\Delta_{j,c}^E/\Delta_{j,e}^E = \frac{C^E}{z_j e D_j/(kT)D^E} \sim \text{Pe}_j/z_j, \quad (3.15)$$

and the ratio of the convective and diffusive terms is

$$\Delta_{j,c}^E/\Delta_{j,d}^E = \frac{n_j^\infty C^E}{D_j C_j^E} \sim \text{Pe}_j, \quad (3.16)$$

where the Péclet number $\text{Pe}_j = u_c \kappa^{-1}/D_j$ is typically very small. The characteristic (microscale) velocity u_c may be estimated by balancing the $O(E\sigma\kappa)$ electrical force (per unit volume) with the $O(u_c\eta/\ell^2)$ Darcy drag force, giving $u_c \sim E\sigma\kappa\ell^2/\eta$. With $E \sim 10^2 \text{ V cm}^{-1}$, $\sigma \sim 1 \text{ } \mu\text{C cm}^{-2}$, $\kappa^{-1} \sim 10^2 \text{ nm}$, $\ell \sim 1 \text{ nm}$, and $\eta \sim 10^{-3} \text{ kg m}^{-1}\text{s}^{-1}$, $u_c \sim 1 \text{ } \mu\text{m s}^{-1}$. Further, with $a \sim 1 \text{ } \mu\text{m}$ and $D_j \sim 10^{-9} \text{ m}^2\text{s}^{-1}$, $\text{Pe}_j \sim 10^{-4}$, indicating that diffusion and electromigration ($z_j \neq 0$) dominate convection. Clearly, for charged species with $z_j \sim 1$, electromigrative fluxes are comparable to diffusive fluxes.

Incremental contributions to the ion fluxes are provided in table 3 for the composite whose asymptotic coefficients are shown in table 1. These confirm that the convective contribution $\Delta_{j,c}^E$ is small, and that the electromigrative contribution $\Delta_{j,e}^E$ approaches the Maxwell value $\Delta_{j,e}^E = -3/2$ for impenetrable (non-conducting) spheres as $|\zeta| \rightarrow 0$. Furthermore, the electromigrative ($\Delta_{j,e}^E$) and diffusive ($\Delta_{j,d}^E$) contributions for Na^+ and Cl^- vary significantly with ionic strength. For example, at low electrolyte concentration, the diffusive term dominates, enhancing the flux of the counterion (Na^+) and attenuating that of the co-ion (Cl^-).

3.5. Electrical conductivity

The electrical conductivity of colloidal dispersions is well known to reflect the particle surface charge density (Russel *et al.* 1989). The conductivity of a composite with immobilized particles presents a relatively simple problem when the electrolyte ions are unhindered by the polymer, because only the electrolyte ions—not the charge on the particles (macroions) themselves—contribute to charge transfer. This section establishes whether the electrical conductivity is sensitive to the surface charge and, possibly, the permeability of the polymer-gel.

From the fluxes in Eqn. (3.2), the average current density may be written

$$\mathbf{I} = \sum_{j=1}^N z_j e \mathbf{J}_j \approx K^\infty \mathbf{E} + \phi(3/a^3) \mathbf{E} [K^\infty D^E + \sum_{j=1}^N z_j e D_j C_j^E], \quad (3.17)$$

where

$$K^\infty = \sum_{j=1}^N (z_j e)^2 D_j / (kT) n_j^\infty \quad (3.18)$$

is the conductivity of the electrolyte. The conductivity of the composite is defined as

$$K^* = I/E = K^\infty (1 + \phi \Delta^K), \quad (3.19)$$

TABLE 3. Incremental contributions (see Eqn. (3.14)) to the bulk *electromigration* of NaCl in a Brinkman medium with charged spherical inclusions: $a = 100$ nm; $\ell \approx 0.951$ nm; $T = 25^\circ\text{C}$; $D_1 \approx 1.33 \times 10^{-9} \text{m}^2\text{s}^{-1}$ (Na^+); $D_2 \approx 2.03 \times 10^{-9} \text{m}^2\text{s}^{-1}$ (Cl^-).

$\zeta e/(kT)$	$\Delta_{j,e}^E$ ($j = 1, 2$)	$\Delta_{1,d}^E$ (Na^+) ($= -\Delta_{2,d}^E$)	$\Delta_{1,c}^E$ (Na^+)	$\Delta_{2,c}^E$ (Cl^-)	Δ_1^E (Na^+)	Δ_2^E (Cl^-)	Δ^K
$\kappa a = 1$	$I = 9.25 \times 10^{-6} \text{ mol l}^{-1}$						
-1	-1.15×10^0	6.25×10^0	-2.17×10^{-4}	1.42×10^{-4}	5.10×10^0	-7.39×10^0	-2.44×10^0
-2	-1.71×10^{-1}	1.22×10^1	-4.25×10^{-4}	2.78×10^{-4}	1.21×10^1	-1.24×10^1	-2.72×10^0
-4	$+2.60 \times 10^0$	2.23×10^1	-7.70×10^{-4}	5.05×10^{-4}	2.49×10^1	-1.97×10^1	-2.05×10^0
-6	$+4.79 \times 10^0$	2.86×10^1	-9.74×10^{-3}	6.38×10^{-4}	3.34×10^1	-2.39×10^1	-1.16×10^0
-8	$+5.89 \times 10^0$	3.17×10^1	-1.05×10^{-3}	6.87×10^{-4}	3.76×10^1	-2.58×10^1	-6.91×10^{-1}
$\kappa a = 10$	$I = 9.25 \times 10^{-4} \text{ mol l}^{-1}$						
-1	-1.42×10^0	4.38×10^{-1}	-1.39×10^{-3}	9.12×10^{-4}	-9.85×10^{-1}	-1.86×10^0	-1.51×10^0
-2	-1.19×10^0	9.08×10^{-1}	-2.81×10^{-3}	1.84×10^{-3}	-2.88×10^{-1}	-2.10×10^0	-1.38×10^0
-4	-4.11×10^{-1}	1.95×10^0	-5.36×10^{-3}	3.52×10^{-3}	$+1.53 \times 10^0$	-2.35×10^0	-8.16×10^{-1}
-6	$+3.96 \times 10^{-1}$	2.86×10^0	-6.32×10^{-3}	4.14×10^{-3}	$+3.25 \times 10^0$	-2.46×10^0	-1.98×10^{-1}
-8	$+8.84 \times 10^{-1}$	3.38×10^0	-5.45×10^{-3}	3.57×10^{-3}	$+4.26 \times 10^0$	-2.50×10^0	$+1.81 \times 10^{-1}$
$\kappa a = 100$	$I = 9.25 \times 10^{-2} \text{ mol l}^{-1}$						
-1	-1.49×10^0	4.70×10^{-2}	-8.08×10^{-3}	5.30×10^{-3}	-1.45×10^0	-1.53×10^0	-1.50×10^0
-2	-1.45×10^0	1.08×10^{-1}	-1.64×10^{-2}	1.08×10^{-2}	-1.36×10^0	-1.54×10^0	-1.47×10^0
-4	-1.23×10^0	3.35×10^{-1}	-3.33×10^{-2}	2.18×10^{-2}	-9.31×10^{-1}	-1.55×10^0	-1.30×10^0
-6	-7.59×10^{-1}	8.11×10^{-1}	-4.44×10^{-2}	2.91×10^{-2}	$+7.38 \times 10^{-3}$	-1.54×10^0	-9.27×10^{-1}
-8	-1.14×10^{-1}	1.46×10^0	-4.15×10^{-2}	2.72×10^{-2}	$+1.30 \times 10^0$	-1.55×10^0	-4.17×10^{-1}

where Δ^K is termed the (dimensionless) *conductivity increment*.

Equations (3.17)-(3.19) are equivalent to expressions derived by O'Brien (1981) for the conductivity of dilute colloidal dispersions with the particles undergoing electrophoresis. Here, the asymptotic coefficients are different because the particles are stationary[†]. When the ζ -potential is low and, hence, ion fluxes are unperturbed by the surface charge, the dipole strength for non-conducting spheres equals the Maxwell value $D^E = -(1/2)a^3$, so $\Delta^K \rightarrow -3/2$ as $|\zeta| \rightarrow 0$. In general, however, the conductivity increment also reflects the charge of the inclusions *and* the ionic strength.

Similarly to dispersions, the average convective term (involving C^E in Eqn. (3.2)) does not influence the conductivity increment (because of electrical neutrality), and the diffusive term (involving C_j^E) vanishes only when the species have equal mobilities. In general, the (microscale) electromigrative and diffusive terms (involving D^E and C_j^E) contribute to the average current density. However, because these are influenced by fluid motion, the conductivity of a composite is not the same as when particles are fixed in an electrolyte without polymer. As expected, because only the electrolyte ions contribute to charge transfer, the conductivity of a composite is lower than when particles undergo electrophoresis.

Representative conductivity increments for mobile (*solid lines*) and stationary (*dashed lines*) particles in a NaCl electrolyte without polymer are compared in figure 6[‡]. At low ionic strength (small κa), immobilizing the particles decreases the conductivity increment, because particle migration (electrophoresis) contributes significantly to charge transfer. At high ionic strength ($\kappa a > 10$), however, the conductivity increments for mobile and fixed particles are (practically) the same. This is because the density of charge added by the particles (macroions) is vanishingly small compared to the density of bulk electrolyte ions, so the conductivity reflects only the contribution of (dielectric and double-layer) polarization to the average electric field.

In contrast to KCl and HClO₄ electrolytes (see O'Brien 1981), the conductivity increment with NaCl *decreases* with increasing ζ -potential when ζ and κa are small. This may be attributed the counterion (Na⁺) having a significantly lower mobility than the co-ion (Cl⁻). For KCl, the mobilities of K⁺ and Cl⁻ are very similar, yielding a monotonically increasing conductivity increment. For HClO₄, however, the counterion (H⁺) has a significantly higher mobility than the co-ion (ClO₄⁻), yielding a conductivity increment that *increases* more rapidly (linearly) with $|\zeta|$ (see O'Brien 1981).

The conductivity increment for particles with radius $a = 100$ nm embedded in a polymer gel with Brinkman screening length $\ell \approx 3.11$ nm (*solid lines*) is shown in figure 7. Similar calculations (not shown) reveal that an order-of-magnitude increase in the permeability ℓ^2 produces almost the same values at all ζ -potentials and ionic strengths (values of κa). This confirms that the average current density is dominated by electromigration and diffusion. The conductivity increments (*solid lines*) are compared to values for stationary particles in an electrolyte without polymer (*dashed lines*). These results are almost the same at high ionic strength when the diffuse double layer is thin compared to the Brinkman screening length, *i.e.*, when $\kappa \ell \gg 1$. Under these conditions, the electrical force (inside the diffuse double layer) is balanced by viscous stress and, hence, the convective flows are similar. When $\kappa \ell = \kappa a(\ell/a) = 1$, for example, $\kappa a \approx 100/3.11 \approx 32$

[†] When particles undergo electrophoresis in a Newtonian electrolyte, the far-field (solenoidal) velocity disturbance is irrotational, decaying as r^{-3} as $r \rightarrow \infty$. When *fixed* in electrolyte without polymer, however, the far-field disturbance reflects a net force, decaying as r^{-1} as $r \rightarrow \infty$.

[‡] The computations for particles in a pure electrolyte were performed with software (called MPEK, available from the author) based on the work of Hill *et al.* (2003). These accurately reproduced earlier calculations by O'Brien (1981) for KCl and HClO₄ electrolytes.

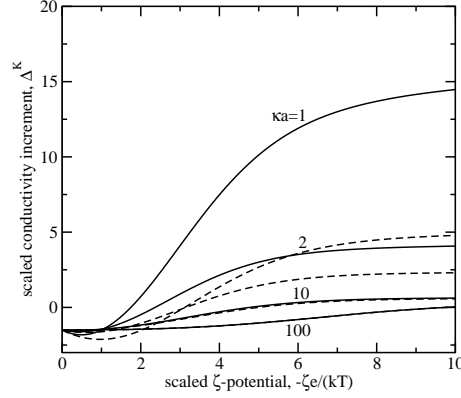


FIGURE 6. The (scaled) conductivity increment Δ^K (see Eqn. (3.19)) as a function of the (scaled) ζ -potential $\zeta e/(kT)$ for various (scaled) reciprocal double-layer thicknesses $\kappa a = 1, 2, 10$ and 100 (aqueous NaCl at $T = 25^\circ\text{C}$ with $a = 100$ nm) for particles undergoing electrophoresis (*solid lines*) and stationary particles (*dashed lines*), both in electrolyte without polymer.

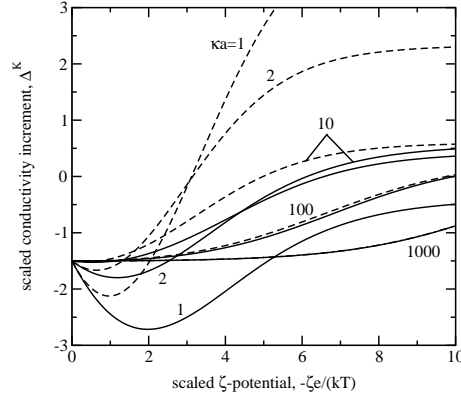


FIGURE 7. The (scaled) conductivity increment Δ^K (see Eqn. (3.19)) as a function of the (scaled) ζ -potential $\zeta e/(kT)$ for various (scaled) reciprocal double-layer thicknesses $\kappa a = 1, 2, 10, 100$ and 1000 : aqueous NaCl at $T = 25^\circ\text{C}$; $a = 100$ nm; $\ell \approx 3.11$ (*solid lines*); stationary particles in electrolyte without polymer (*dashed lines*).

and, as expected, the limiting behavior ($\kappa\ell \gg 1$) at high ionic strength occurs when κa exceeds this value.

4. Summary

A rigorous theoretical methodology was developed to calculate steady electrokinetic transport of electrolytes in a continuous polymer gel embedded with charged spherical inclusions. These composites are promising candidates for enhanced gel-electrophoresis,

chemical sensing, membrane separation, and, perhaps, electroosmotic pumping technologies. This work was also motivated by a desire to interpret experiments that probe the surface charge of immobilized colloidal particles and the micro-rheology of delicate polymer gels.

From a numerically exact treatment of electromigrative, diffusive and convective transport around a single inclusion in an unbounded polymer gel, averaged equations describing bulk transport properties were derived. The theory was applied to calculate the response to a steady electric field with uniform bulk electrolyte concentration. Note that the response to bulk electrolyte concentration gradients is treated in an accompanying paper. In general, electromigration and diffusion were found to be independent of convection and, hence, of the polymer-gel (Darcy) permeability. However, the strength of electroosmotic flow reflects the gel permeability and, to a lesser (but still significant) extent, polarization and relaxation by electromigration and diffusion.

When particles are immobilized in a polymer gel, the electrical conductivity is independent of the polymer, whereas the pore mobility—similarly to the electrophoretic mobility of dispersions—reflects the size and charge of the inclusions, *and* the Darcy permeability. Furthermore, when the Debye length is smaller (greater) than the Brinkman screening length ℓ (square root of the Darcy permeability), the pore mobility increases linearly (quadratically) with ℓ .

The variation of the pore mobility with ζ -potential and ionic strength is more complicated, because of the significant influence of polarization and relaxation. Nevertheless, the mobility is (approximately) inversely proportional to the inclusion radius, indicating, as expected, that the average flow is proportional to the average counter-charge density.

The Darcy drag of the intervening polymer gel leads to slow flows that will often be independent of the differential pressure required to pump fluid through a (modest) microfluidic network. Optimal pumping efficiency is favored by thin membranes with large cross-section, high inclusion volume fractions, and low electrolyte conductivities.

The present model assumes that the polymer gel does not influence ion mobilities (diffusion coefficients), and that the volume fraction of the inclusions is small. By analogy with Maxwell's well-known theory for conduction in dilute random arrays of spheres, the theory may also be accurate at moderate volume fractions. Note also that the calculations require the bulk electrostatic potential and electrolyte ion concentrations to vary slowly in space (and time). Future development of the model will accommodate harmonic temporal fluctuations in the applied electric field, permitting the interpretation of dielectric relaxation spectroscopy experiments.

Supported by the Natural Sciences and Engineering Research Council of Canada (NSERC), through grant number 204542, and the Canada Research Chairs program (Tier II). The author thanks S. Omanovic and J. Vera (McGill University) and I. Ispolatov (University of Santiago) for fruitful discussions related to this work.

REFERENCES

- BOOTH, F. 1950 The cataphoresis of spherical, solid non-conducting particles in a symmetrical electrolyte. *Proc. Roy. Soc. Lond.* **203**, 533–551.
- DELACEY, E. H. B. & WHITE, L. R. 1981 Dielectric response and conductivity of dilute suspensions of colloidal particles. *J. Chem. Soc., Faraday Trans. 2* **77**, 2007–2039.
- DUKHIN, S., ZIMMERMAN, R. & WERNER, C. 2004 Intrinsic charge and Donnan potentials of grafted polyelectrolyte layers determined by surface conductivity data. *J. Colloid and Interface Sci.* **274** (1), 309–318.
- HILL, R. J. 2004 Hydrodynamics and electrokinetics of spherical liposomes with coatings of

- terminally anchored poly(ethylene glycol): Numerically exact electrokinetics with self-consistent mean-field polymer. *Phys. Rev. E* **70**, 051046.
- HILL, R. J. & SAVILLE, D. A. 2005 ‘exact’ solutions of the full electrokinetic model for soft spherical colloids: Electrophoretic mobility. *Colloids and Surfaces A: Physiochemical and Engineering Aspects* .
- HILL, R. J., SAVILLE, D. A. & RUSSEL, W. B. 2003 Electrophoresis of spherical polymer-coated colloidal particles. *J. Colloid Interface Sci.* **258**, 56–74.
- HUNTER, R. J. 2001 *Foundations of Colloid and Interface Science*, 2nd edn. Oxford University Press.
- KOCH, D. L. & SANGANI, A. S. 1999 Particle pressure and marginal stability limits for a homogeneous monodisperse gas fluidized bed: Kinetic theory and numerical simulations. *J. Fluid Mech.* **400**, 229–263.
- O’BRIEN, R. W. 1981 The electrical conductivity of a dilute suspension of charged particles. *J. Colloid Interface Sci.* **81** (1), 234–248.
- O’BRIEN, R. W. 1988 Electro-acoustic effects in a dilute suspension of spherical particles. *J. Fluid Mech.* **190**, 71–86.
- O’BRIEN, R. W. 1990 The electroacoustic equations for a colloidal suspension. *J. Fluid Mech.* **212**, 81–93.
- O’BRIEN, R. W. & WHITE, L. R. 1978 Electrophoretic mobility of a spherical colloidal particle. *J. Chem. Soc., Faraday Trans. II* **74**, 1607–1626.
- RUSSEL, W. B., SAVILLE, D. A. & SCHOWALTER, W. R. 1989 *Colloidal Dispersions*. Cambridge University Press, paperback edition 1991.
- SAVILLE, D. A. 1979 Electrical conductivity of suspensions of charged particles in ionic solutions. *J. Colloid Interface. Sci.* **71** (3), 477–490.
- SAVILLE, D. A. 1982 The sedimentation potential in a dilute suspension. *Adv. Colloid Interface Sci.* **16** (1), 267–279.
- SAVILLE, D. A. 2000 Electrokinetic properties of fuzzy colloidal particles. *J. Colloid Interface Sci.* **222**, 137–145.
- YAO, S., HERTZOG, D. E., MIKKELSEN, J. C. J. & SANTIAGO, J. G. 2003 Porous glass electroosmotic pumps: design and experiments. *J. Colloid Interface Sci.* **268**, 143–153.
- YAO, S. & SANTIAGO, J. G. 2003 Porous glass electroosmotic pumps: theory. *J. Colloid Interface Sci.* **268**, 133–142.